

# Acoustic shock wave-induced short-range ordered graphitic domains in amorphous carbon nanoparticles and correlation between magnetic response and local atomic structures

Sivakumar Aswathappa<sup>a</sup>, Lidong Dai<sup>a,\*</sup>, Sahaya Jude Dhas Sathiyadhas<sup>b</sup>,  
Martin Britto Dhas Sathiyadhas Amalpushpam<sup>c</sup>, Muthuvel Vijayan<sup>d</sup>, Ikhyun Kim<sup>e</sup>,  
Raju Suresh Kumar<sup>f</sup>, Abdulrahman I. Almansour<sup>f</sup>

<sup>a</sup> Key Laboratory of High-temperature and High-pressure Study of the Earth's Interior, Institute of Geochemistry, Chinese Academy of Sciences, Guiyang, Guizhou 550081, China

<sup>b</sup> Department of Physics, Kings Engineering College, Sriperumbudur, Chennai, Tamilnadu 602 117, India

<sup>c</sup> Shock Wave Research Laboratory, Department of Physics, Abdul Kalam Research Center, Sacred Heart College, Tirupattur, Tamil Nadu 635 601, India

<sup>d</sup> Department of Physics, School of Foundation Science, Kumaraguru College of Technology, Coimbatore, Tamilnadu 641 049, India

<sup>e</sup> Department of Mechanical Engineering, Keimyung University, Daegu 42601, Republic of Korea

<sup>f</sup> Department of Chemistry, College of Science, King Saud University, P.O. Box 2455, Riyadh 11451, Saudi Arabia

## ARTICLE INFO

### Keywords:

Amorphous carbon  
Shock waves  
Graphitization  
Magnetic properties

## ABSTRACT

Over the years, a wide range of spectral research has been carried out on various carbon forms to explore deeply their structure-property relationship. The structural stability of carbon allotropes remains to be a challenging endeavor yet to be achieved under extreme conditions, especially under acoustical shocked conditions. From the experimental findings, we report the acoustic shock wave response of the amorphous carbon nanoparticles and the resultant degree of crystalline nature, morphological characteristics and magnetic response. Moreover, analytical techniques such as X-ray diffractometry (XRD), Raman spectrometer, High resolution transmission electron microscopy (HR-TEM) and vibrational sample magnetometer (VSM) have been employed to arrive at the relationships of structure – morphology – magnetic properties under shocked conditions. Interestingly, under shocked conditions (0, 250, 500 and 750 shocks), compelling evidence has been found for the short-range amorphous pockets which turn into spatially short-range ordered graphitic domains within the sphere-shaped amorphous nanoparticles whereby the obtained values of the ratio  $I_D/I_G$  of the samples are 0.94, 0.93, 0.95 and 1.01 for 0, 250, 500 and 750 shocked conditions, respectively. Moreover, the saturation magnetization is found to have reduced in the base of the local atomic ordering and the obtained values are found to be 1, 0.64, 0.41, 0.725 emu/g for 0, 250, 500 and 750 shocked conditions, respectively. The structure-property relationship is to be elaborated in the upcoming sections.

## 1. Introduction

The studies on atomic ordering and disordering in solids provide a considerable amount of profound knowledge to understand better the functional properties of materials. In order to gain such substantiated knowledge, various environmental extreme conditions are to be explored such that the required potential materials could be identified which would have the potential to withstand their identity while encountering diverse environmental conditions [1–3]. The primary extreme conditions such as static high temperature, high pressure and

gamma rays, as well as laser irradiations are mostly utilized to tune the materials' structures and properties. Among the aforementioned approaches, the static high-temperature and high-pressure compression experiments on solids have a pretty long history of materials research [4,5] while the required scientific information and technological backups for gamma irradiation and laser irradiations are still in the developing stages [6,7]. The numerous results of experiments conducted on static temperature often demonstrate that materials undergo a static–recrystallization process at higher temperatures [8]. Conversely, in the static pressure compression experiments, the ordered structure tends

\* Corresponding author.

E-mail address: [dailidong@vip.gyg.ac.cn](mailto:dailidong@vip.gyg.ac.cn) (L. Dai).

<https://doi.org/10.1016/j.diamond.2023.110587>

Received 25 July 2023; Received in revised form 2 November 2023; Accepted 7 November 2023

Available online 11 November 2023

0925-9635/© 2023 Elsevier B.V. All rights reserved.

to transform into disordered structures via a few crystallographic structural transitions which is the most probable outcome of the static compression experimental results [9,10]. After the advent of the 21st century, dynamic shock waves-assisted experiments in solid-state materials have gained significant prominence in mainstream research such that, after the invention of tabletop shock tubes [11,12], the applications of shock waves have attained a tremendous position whereby the investigation of materials aftermath of exposing to shock waves has emerged as one of the prominent techniques exclusively conducive for extreme environments which fit in Materials Science branch [13–15]. It is imperative to note that a range of structural transitions has been observed in both bulk single crystals and nanocrystals [16–20]. However, it is worth mentioning that certain materials exhibit stable crystal structures under shocked conditions [21,22].

Besides the investigation of functional metal oxide phase transitions under shocked conditions, shock wave-induced transitions on carbon materials have gained considerable attention in recent years due to their spectacular structural transitions arising out of their prevailing unique structural characteristics which promote a higher chance of possessing the potential ability to allotropy transitions [23–28]. Note that carbon exhibits various allotropes such as diamond, graphite, graphene, fullerene, carbon nanotube, amorphous carbon, etc. Extensive research on carbon's behavior under static high-temperature and high pressure has yielded substantial data that have been documented over the last few decades [23–38]. But rather than the existing data on static compression results, the available reports on dynamic acoustical shock waves are minimal. Koteeswara Reddy et al. have demonstrated the traces of diamond-like nanoparticles from the graphitic thin films under acoustical shocked conditions wherein the corresponding shock pressure has been kept at 50 MPa [29] and, on the other hand, the crystalline carbon (C60) is converted into the amorphous phase carbon at the shock temperature of 2540 K [30]. Recently, Arijit Roy et al. have performed shock wave recovery experiments using amorphous carbon NPs [50 (sp<sup>2</sup>):50 (sp<sup>3</sup>)] as starting material and achieved nanoribbons, nano onions, nanotube structures at the shock temperature of 7300 K. Note that the above-mentioned research work [31] has been carried out using a conventional shock tube which can produce very high enthalpy and high-temperature shock waves (in the order of few thousand Kelvin) [1–3]. However, a tabletop shock tube is quite simple such that it is capable of producing weak shock waves of a few hundred Kelvin transient temperature [11–13,17,18]. Despite its simplicity, when the shock waves emanating from the tabletop shock tube are repeatedly applied to samples, comparable results can be achieved as obtained by the conventional shock tubes [31,32]. For example, amorphous multi-wall carbon nanotubes were exposed to shock waves using a tabletop Reddy Tube whereby the respective crystalline material was achieved as the end product at the 300-shocked condition with the transient pressure 1.0 MPa [32].

The current study focuses on conducting a shock wave processing experiment on amorphous carbon nanostructures which is driven by two significant academic and technological motivations. Firstly, amorphous carbon possesses several tetrahedral carbon structures that closely resemble diamond structures. Therefore, by utilizing shock waves, it may be feasible to generate diamond nuclei within amorphous carbon. Shock waves have the capability to induce substantial structural changes in carbon samples, providing a potential avenue for synthesizing diamonds from different carbon forms. This area of research, exploring the synthesis of diamonds from various carbon sources, has been a long-standing and notable topic of investigation [1–4]. The second one is that numerous shock wave experiments have been conducted with the crystalline counterpart of carbon using it as a starting material whereas the information on the phase of amorphous sample's features under shocked conditions remains to be in poor light. Amorphous carbon (a-C) is a carbon synthetic allotrope, made of a mixture of tetrahedral sp<sup>3</sup> (diamond-like) and trigonal sp<sup>2</sup> (graphite-like) which are present in carbon in various ratios [33–35]. A few static pressure experiments have

been carried out to understand the chemistry of amorphous carbon whereby interesting results have been found [36–38]. Analyzing these studies [36–38], it is evident that the combined effect of temperature and pressure is more pronounced for the achievement of phase transitions in carbon rather than them only being treated with the pressure. As a further step to explore these new features of the amorphous carbon materials, the test samples are exposed to shock waves thereby characterizing ex-situ of the effect of the shock waves on the samples. Having performed the experiments, it becomes clear that acoustical shock waves can trigger the amorphous carbon NPs providing impressive results due to the thermal effect along with the pressure. Note that under shocked conditions, it is possible to create the formation of short-range ordered graphitic domains with impressive morphological characteristics and such short-range ordered graphitic domains have greater advantages as against simple amorphous carbon, especially in chemical sensors, optical limiting, catalysis and Li-ion electrochemical energy-storage devices. In addition to that, the present work clearly discloses the potential capability of the tabletop shock tube compared to conventional shock tubes.

### 1.1. Experimental sections

Amorphous carbon nanoparticles (a-C < 50 nm diameter) were purchased (from Carbon NanoMaterials Technology Co., Ltd., South Korea). The amorphous carbon nanoparticles have been subdivided into four equal parts such that one part has been kept as the control sample while the rest of the samples have been utilized for the shock wave-impact analyses. For the experimental analysis, Mach number 2.2 shock waves (with the respective transient pressure and temperature of 2.0 MPa and 864 K) have been preferred such that three different sets of shock pulses with the counts of 250, 500 and 750 shocks have been exposed on those three samples, respectively. The shock waves have been generated utilizing a semiautomatic Reddy Tube (Fig. S1) and a detailed procedure for the measurement of shock parameters [12], as well as shock wave loading procedure, have been described in the previous reports [17,18] and also provided in the supplementary section. After the completion of the shock wave-impact procedures, the shock wave loaded samples and the control sample have been fixed for the respective characterizations of powder X-ray diffraction (XRD), Raman spectroscopic, high resolution transmission electron microscopic (HR-TEM) and vibrating sample magnetometric (VSM) analyses to be carried out.

### 1.2. Instrumentation details

The analytical instruments details are as follows; Powder X-ray diffraction (PXRD) [Rigaku – Smart Lab X-Ray Diffractometer, Japan-CuK $\alpha$  as the X-ray source ( $\lambda = 1.5407 \text{ \AA}$ ), with the step precision of  $\pm 0.001^\circ$ ] analysis was performed. A Renishaw model Raman spectrometer with a Laser line 532 nm of power 50 mW was preferred with which the Raman measurement was carried out using the pelletized form of samples. The laser spot size was  $50 \mu\text{m}^2$  and the optical microscope's objective lens had an X50 long working distance ( $WD = 10.6 \text{ mm}$ ) and the value of numerical aperture was 0.5 while the Raman data was collected by Renishaw Wire 5.1 instrument control and the data acquisition software. Microscopical structural characterizations for the starting and shock-recovered samples were investigated using an HRTEM, which was operated at the State Key Laboratory of Environmental Geochemistry, Institute of Geochemistry, Chinese Academy of Sciences, Guiyang, China. A small amount of sample was homogeneously distributed onto a carbon-film-coated copper grid for the HRTEM observation, which was performed through a Tecnai G2 F20 S-TWIN TMP with an acceleration voltage of 200 kV. The inter-planar spacing of the samples was precisely measured through Digital Micrograph software. A vibrating sample magnetometer (Lake Shore, Cryotronics) was utilized to understand the structural and magnetic

structural stability of the test samples under shocked conditions.

## 2. Results and discussion

### 2.1. XRD results

It is essential to make sure of clear structural details about the control sample's  $sp^3$  and  $sp^2$  ratio before analyzing the actual shock wave-induced changes in the test sample. In Fig. 1, the control amorphous carbon NPs' XRD pattern is presented which has two broad XRD peaks at  $24.65^\circ$  and  $43.20^\circ$  and these two diffraction peak positions belong to the hexagonal structure of the Graphene and Graphite. Moreover, Pseudo-Vigot functions peak fitting is used for a better understanding of the peak profiles such as peak shift and full-width at half maximum. In general, amorphous carbon (purely made of  $sp^3$  carbons) must have a very broad peak between  $20$  and  $25^\circ$  but, in practice, it is very difficult to get pure amorphous carbon structures which is always not possible to get the combination of  $sp^3$  and  $sp^2$  hybridizations such as 80:20, 70:30 or 50:50 amorphous carbons structures. If the amorphous sample has the  $sp^2$  hybridizations (crystalline content) it could be understood that the ultra short-range Graphene layers may appear in the test sample and similar kinds of results have been reported referring to it as amorphous carbon rather than the Glassy carbon [38,39].

Hence, it is quite clear that the control sample has  $sp^3$  and  $sp^2$  hybridizations wherein  $sp^3$  hybridization dominates. As seen in shocked conditions, there could be some changes in terms of peak shift and peak width with respect to the number of shock pulses and these profiles are displayed in Fig. 2. Note that, in the control sample, the broad XRD peak of (002) is located at  $24.65^\circ$  whereas, under shocked conditions, it got shifted towards the higher diffraction angle to be located at  $25.14$ ,  $25.87$

and  $25.39$  for the respective shocked conditions of 250, 500 and 750 which clearly indicates that at 250 and 500 shocked conditions, there might have lattice compression happened while under 750 shocked condition, lattice deformations could have taken place. Thus, it is authenticated that the compression linearly increases while increasing the number of shock pulses from 0 to 500 and further increasing, it starts to undergo structural deformations which may be due to the existence of higher transient pressure and temperature effects. In general carbon crystallography, if a structure undergoes significant lattice compression, there is a high possibility for the formation of graphene or graphite structures. The crystalline graphene layer structured in the (002) plane position is  $26.00$  degrees [40] and the graphite layer structured in the (002) plane position is  $26.44$  degrees (JCPDS: 12-0212) [41]. Graphite is a highly compressed state of graphene layers such that it has lesser crystal volume compared to graphene which is reflected in the difference found in the respective peak position of the graphite and graphene. Based on the previous results, it is quite obvious that, under shocked conditions, the short-range ordered graphitic domains are formed for which the clinching evidence is found in the upcoming HR-TEM results. The short-range ordered graphitic domains are formed along the c-axis under shocked conditions [31] which may be due to the reduction of a few partial  $sp^3$  hybridizations being converted into the  $sp^2$  hybridizations that facilitate the artificial nucleation sites in the amorphous carbon and such sites actually induce the formation of short-range ordered graphitic domains [42].

In addition to that, the initial amorphous phase has quite a highly dense phase like that of the diamond phase because of the presence of the  $sp^3$  tetrahedrons [31]. But, under shocked conditions, the values of full-width at half maximum for the peaks are found to have increased which may be due to the reduction of dense  $sp^3$  hybridizations. The

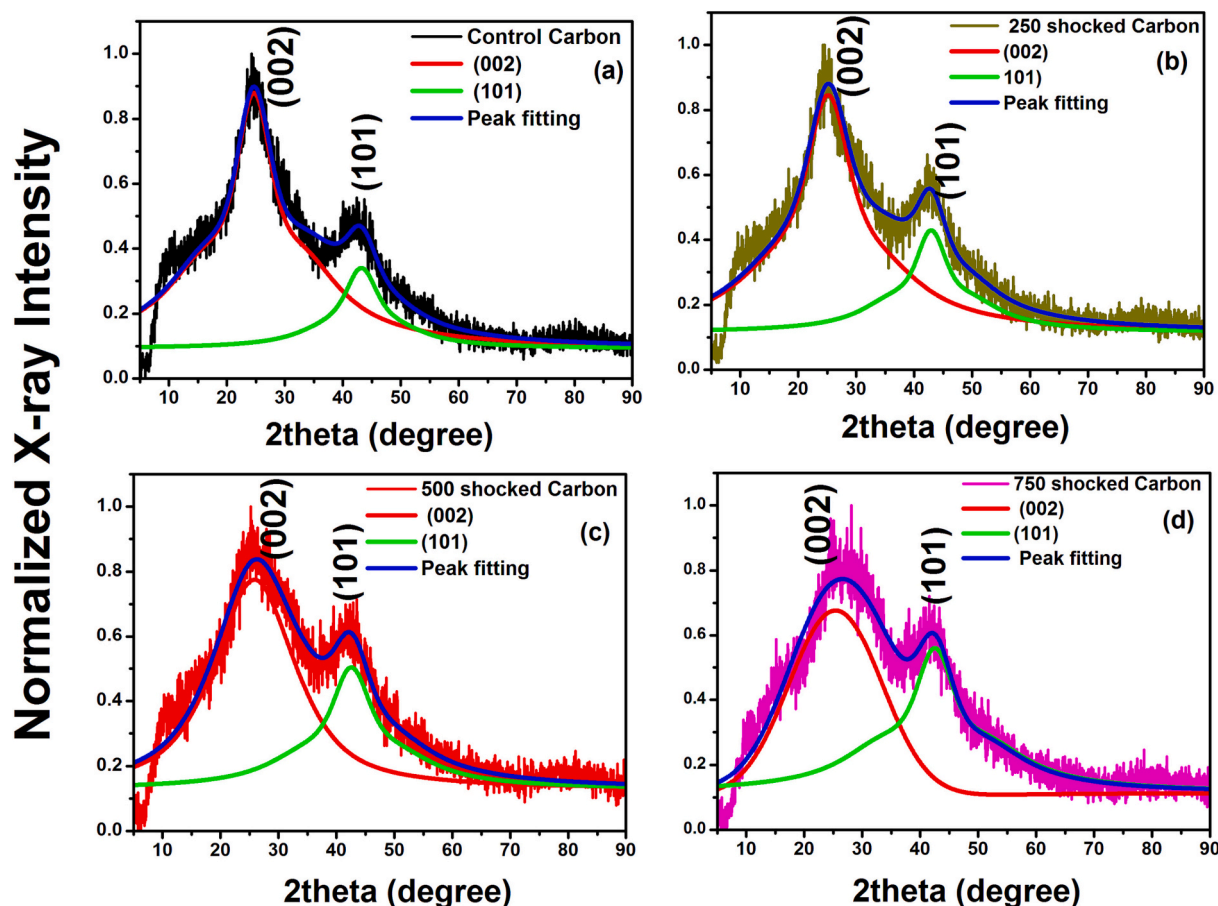


Fig. 1. The XRD patterns of the control and shocked amorphous carbon samples.

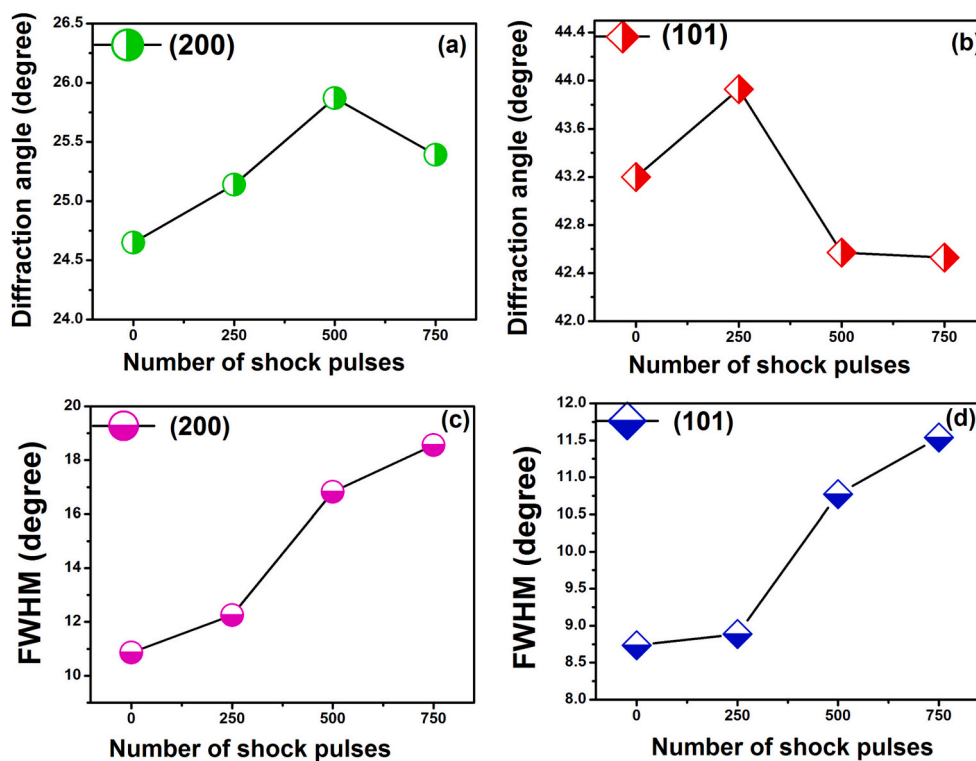


Fig. 2. (a, b) peak shift and (c, d) FWHM profiles of the control and shocked amorphous carbon samples obtained by Pseudo-Vigot functions peak fittings.

amorphous carbons prepared at lower temperatures are supposed to have a high concentration of non-graphitizable species with stronger  $sp^3$  bonds, whereas under shocked conditions, a few of the graphitizable species are easily crystallized into the graphene (or) graphite structures because of the dynamic re-crystallization process, but instead, more unlikely to be converted into diamond [38]. As discussed earlier, the combined effect of pressure and temperature is highly favorable to initiate the crystallization process in carbon materials [38] and hence, under acoustic shocked conditions, interesting results could be highly possible in carbon materials due to the combined effect of transient pressure and temperature [32].

On the other hand, the (101) plane does not reflect much changes in terms of the peak shift with respect to the number of shock pulses which may be due to the high stability of the plane as it connects with the axes of a and c. But in the case of the (002) plane, the buckling and puckering mechanism can be easily triggered by external sources such as high pressure and temperature [43,44]. In addition to that, when the  $sp^3$ -bonded C atoms are dominant in the local atomic structure, it is almost similar to the cubic diamond structure and hence the mechanical hardness, structural stability and tribological properties are reasonably high. Because of the high mechanical and structural strength of the amorphous carbon particles, the applied shock pressure and temperature may not be sufficient to enforce the transition from amorphous carbon to crystalline carbon [43,44] (graphene and graphite) such that it is extremely tough to complete the conversion process of the amorphous carbon particles into the short-range ordered graphitic domains. Followed by the results of diffraction peak position of the (002) plane, the full-width at half maximum (FWHM) of the samples also pronounce impressive results under shocked conditions and the values are identified to be 10.255, 12.250, 16.825, and 18.560 for the 0, 250, 500 and 750 shocked conditions, respectively. Note that the value of FWHM is increased at the 250, 500 and 750-shocked conditions which may be because of short-range ordered graphitic domains that have undergone significant lattice stress by the impact of shock waves.

## 2.2. Raman spectral results

The amorphous samples were subjected to the Raman spectral studies to understand the Raman signature band features under shocked conditions such that the obtained Raman spectra are shown in Fig. 3 wherein the control amorphous carbon sample has two active Raman bands positioned at  $1341.9\text{ cm}^{-1}$  and  $1572\text{ cm}^{-1}$  which are ideally represented as D-band (disordered  $sp^2$ ) and G-band ( $E_g$  symmetry mode - ordered- $sp^2$ ). These Raman bands carry information about the disorder-induced large density of phonon states and in-layer atomic displacement of graphite. The observed Raman band positions are found to have well-matched with the previously reported amorphous carbon samples [31]. Note that, as discussed in the XRD section, the appearance of the Raman active band (G band) clearly illustrates that an adequate number of  $sp^2$  hybridizations are present in the control amorphous. Herein, the processed Pseudo-Vigot functions peak fittings could enable a better understanding of the peak profiles such as peak shift and full-width at half maximum of the D and G bands. Under shocked conditions, the observed results are very impressive in understanding the formation of the short-range ordered graphitic domains under shocked conditions with respect to D and G bands.

The obtained D-band positions for the control and shocked samples are  $1341.9, 1346.9, 1346.0$  and  $1346.7\text{ cm}^{-1}$  for 0, 250, 500, and 750-shocked conditions, respectively. According to the observed Raman shift values of the D band which experiences the positive Raman shift with respect to number of shock pulses which clearly illustrates that a few of the disordered  $sp^2$  hybridizations might have turned into the ordered  $sp^2$  hybridizations that could have led to the formation of the graphene layered structures under shocked conditions [32,45,46]. It's worth noting that Arijit Roy et al. have examined the same kind of amorphous carbon nanoparticles under shocked conditions using a conventional shock tube wherein the shock wave parameters were maintained with Mach number 5.6 and transient temperature 7300 K, respectively such that the un-shocked and shocked D-band positions were  $1348\text{ cm}^{-1}$  and  $1350\text{ cm}^{-1}$ , respectively and the observed band shift difference was  $2\text{ cm}^{-1}$  [31]. Impressively, in the present experiment, the maximum

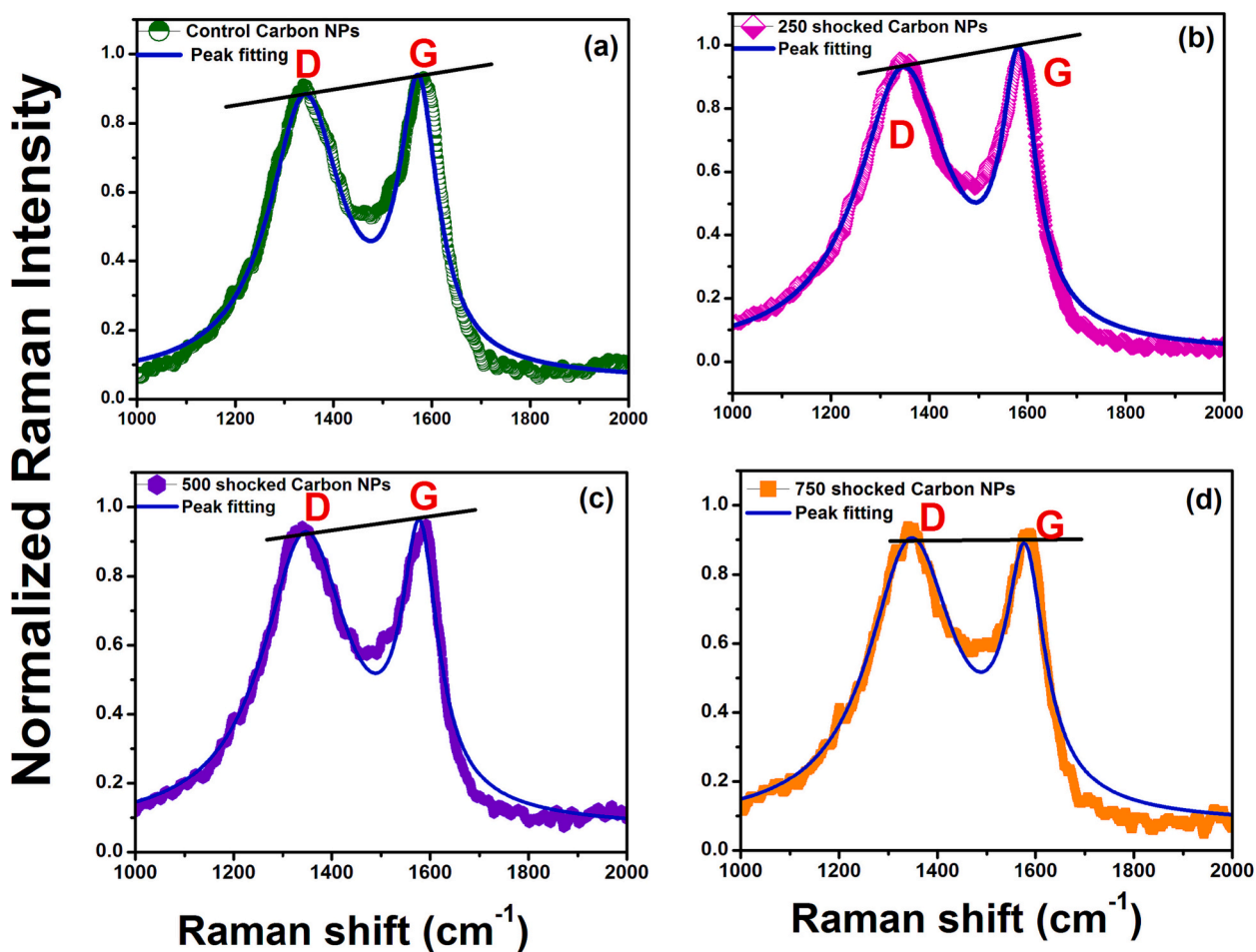


Fig. 3. Raman band features of the control and shocked amorphous carbon samples.

Raman shift difference of  $4.8 \text{ cm}^{-1}$  is achieved at 750 shocked conditions using a tabletop pressure-driven shock tube wherein the transient shock temperature is 864 K. Based on the observed D-band higher shift under shocked conditions, it is evident that the local atomic ordering is enhanced by the impact of shock waves. On the other hand, the G-band

also shows a similar kind of positive Raman band shift features under 250 shocked conditions and is slightly reduced on further increasing the shock numbers and the obtained Raman band locations are 1572, 1582, 1585 and  $1578 \text{ cm}^{-1}$  for the 0, 250, 500 and 750 shocked conditions, respectively. Note that, like that of the D-band, the positive Raman band

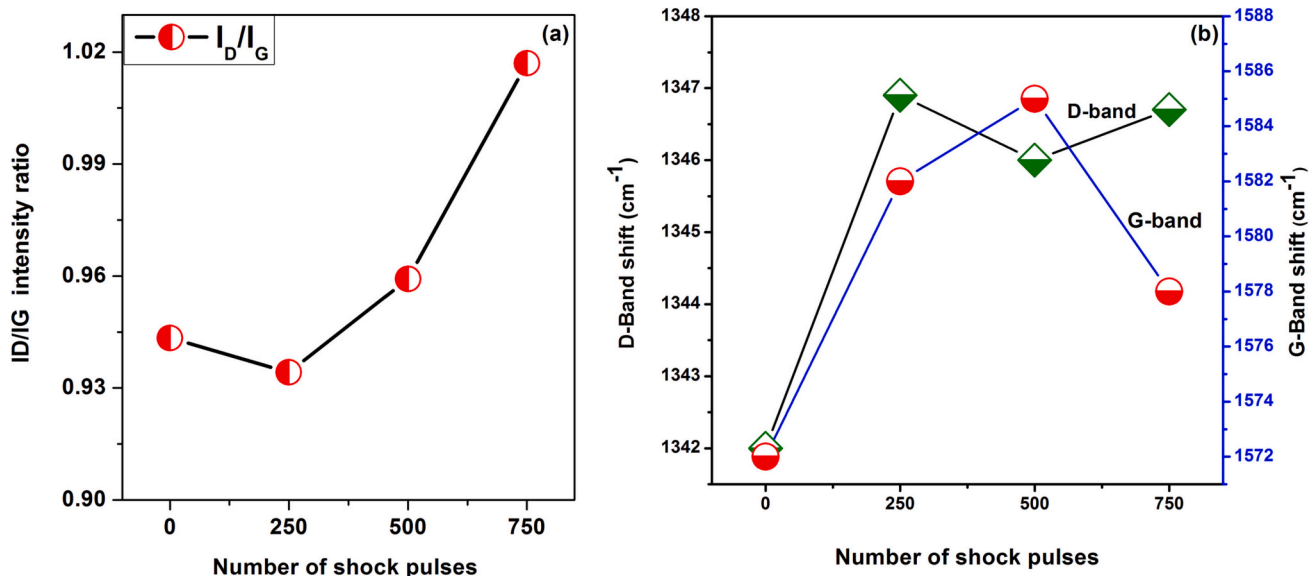


Fig. 4. (a)  $I_D/I_G$  ratio and (b) D-band, G-band shift profiles for the control and amorphous samples against the number of shock pulses.

shift could be found under shocked conditions and it could be clearly illustrated that the net ordered  $sp^2$  hybridization carbon bonds are higher than that of the control sample. The calculated values of  $I_D/I_G$  ratio,  $I_D$  and  $I_G$  band shift of the control and shocked sample are presented in Fig. 4. As seen in Fig. 4a, the  $I_D/I_G$  ratio has slightly reduced at the 250-shocked condition and on further increasing to 500 and 750 shocked conditions, it may lead to changes occurring in the particle size [31]. In general, the  $I_D/I_G$  intensity must be lower for the highly crystalline carbon specimen [35].

Based on this relation, the reduction of the D peak indicates the local ordering of the short-range ordered graphitic domains. As seen in Fig. 4a, it is probable to understand that, under the shocked conditions, there is a slight enhancement of the local ordering which leads to the formation of short-range ordered graphitic domains and the obtained

results are corroborated with the XRD profiles of the present experiment as well as the previous reports of shocked amorphous carbon samples [31]. The overall Raman spectral results represent a possible formation of short-range ordered graphitic domains in the amorphous carbon structures which occurs under shocked conditions. While under acoustical shock wave-loaded conditions, the highly intense energy pulse possessing high pressure and temperature tries to break the potential energy of the surface of the subjected particles within a time span of milliseconds, and in the present case, the test sample of the amorphous carbon has non-graphitizable and graphitizable species on the surface under shocked conditions while the graphitizable species are converted into short-range ordered graphitic domains. In addition to that, the theory and experimental results authenticate that the free electron density is a driving parameter that induces the structural transitions in

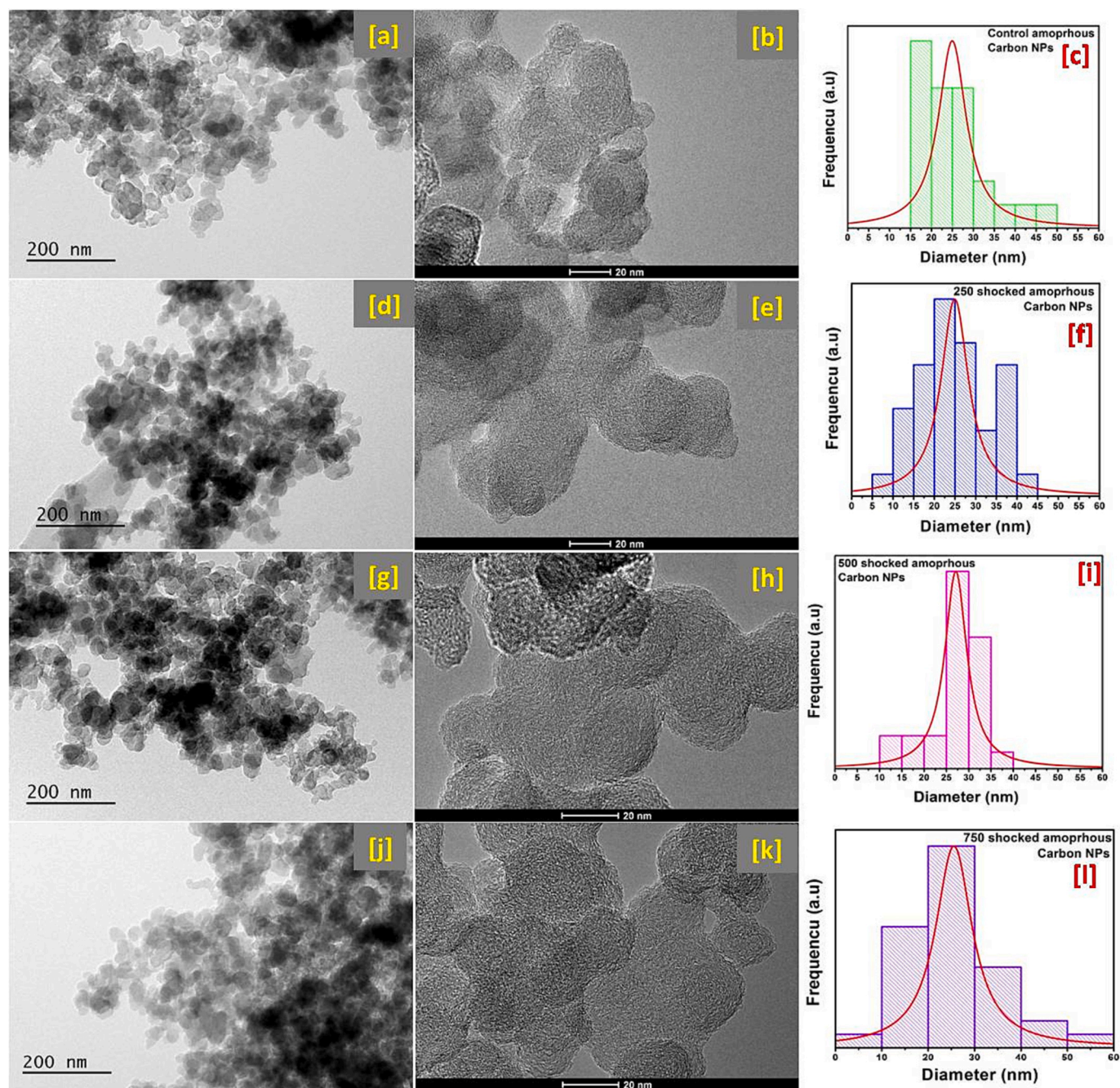


Fig. 5. HR-TEM images and histogram profiles of the control and shocked amorphous carbon samples: the control sample (a–c), 250-shocked sample (d–f), 500-shocked sample (g–i), and 750-shocked sample (j–l).

the case of pure thermal and non-thermal phase transitions in covalent materials such as carbon [47]. A minimum value of around 10 % of the valence band electrons is required for a non-thermal process to initiate the phase transitions and for the thermally assisted process, the required amount of valence electrons may be less than that of the non-thermal process. In the case of the amorphous carbon sample, the minimum free-electron density is known to be  $N_e \sim 4 \times 10^{22} \text{ cm}^{-3}$  which is highly adequate to make the phase transitions process under shocked conditions [47].

### 2.3. High resolution transmission electronic microscopic results

High resolution transmission electron microscopic (HR-TEM) evidence is highly required to understand better the formation of short-range ordered graphitic domains from the amorphous carbon structures under shocked conditions such that the HR-TEM images and histogram profiles are presented in Fig. 5. As reflected in Fig. 5(a–c), the control amorphous sample has particles of spherical shape which have a particle size ranging from 15 to 50 nm wherein most of the particles belong to the region of size 15–30 nm. The calculated values of the average particle size are 24, 25, 25, and 26 nm for 0, 250, 500 and 750 shocked samples, respectively. Based on the obtained values, it seems that the average particle size remains almost constant for the control and shocked samples. Note that, in the case of the control sample, the absence of the long-range order is one of the convincing shreds of evidence for the amorphous nature. On the other hand, due to the presence of short-range atomic ordering in the amorphous sample, it has very low

percentage of the ordered graphitic layers within the spheres [31]. Under shocked conditions, considerable changes could be witnessed in the particle size and local atomic structures such as the formation of the structures of graphitic layers as reflected in Figs. 5 and 6.

The applied supersonic shock waves, while traveling through the test samples, carry a high-temperature enthalpy such that the existing temperature (864 K) and time are sufficient enough to crystallize i.e. the prevalent disordered carbon atoms are transformed into the ordered carbon atoms which is based on the shock wave-induced hot-spot nucleation mechanism [31]. At this point, artificial nucleation takes place, leading to the formation of various carbon nanostructures such as graphite, graphene, MWCNT, fullerene, and other carbon materials [31,32,42]. At this stage, the diffusional reconstructive process can occur such that long-range ordered NPs of short-range ordered graphitic domains are produced under shocked conditions. Note that, the artificial nucleation process is highly sensitive to temperature and pressure and hence with respect to the number of shock pulses, it is possible to get different aspects of results on the formation of short-range ordered graphitic domains under shocked conditions and their respective degree of graphitization [32]. Based on the obtained histogram profiles (Fig. 5c, f, i, and l) of the control and shocked samples, it is quite clear that the particle sizes are varied under shocked conditions because of the shock wave-induced dynamic crystallization occurring within the order of milliseconds. To ensure the reader's benefit as well as to garner a concrete understanding of the obtained shock wave-induced short-range ordered graphitic domains, high resolutions images along with their FFT patterns are provided for the 0, 250, 500 and 750 shocked amorphous

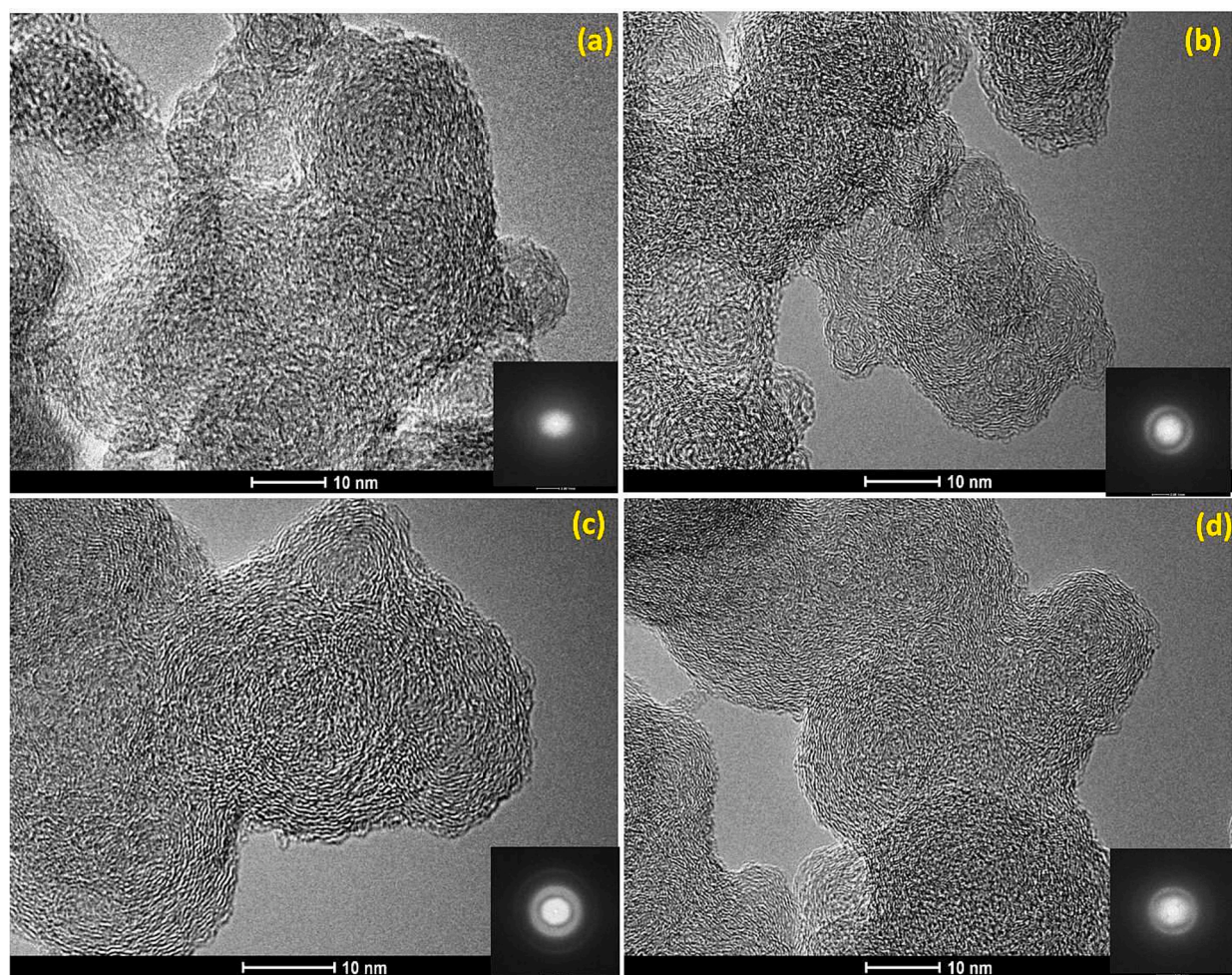


**Fig. 6.** HR-TEM image of the control and shocked amorphous carbon samples (a) the control (b) 250 shocked (b) 500 shocked (c) 750 shocked conditions (inserts: corresponding FFT patterns).

carbon samples in Fig. 6 and the respective zoomed-in portions are presented in Figs. S2–5. The Zoomed-in images, Image J software is used to enrich the visual understanding of the formation of short-range ordered graphitic domains under shocked conditions.

Note that Fig. 6 is provided with 10 nm resolutions of HR-TEM image and for further clarity and as seen in the 250-shocked sample, the outer regions of the spheres have layered structures with the same spherical shape wherein the center part of the sphere has a disordered lattice arrangement. From the TEM images, it is quite clear that, the shock wave impact on the amorphous carbon is highly pronounced on the particle's outer surface whereas, in the inside of the particles, shock wave scattering has occurred due to the presence of a large number of internal grain boundaries between  $sp^2$  and  $sp^3$  carbons. The graphitizable species can be easily formed on the outer surface in the form of  $sp^2$  hybridizations of carbons and the rest of the particles remain to be in the same orbital configurations such that while increasing the shock numbers to 500, more pronounced short-range ordered graphitic domains could be found compared to 250-shocked condition which may be due to the cumulative temperature and pressure effects of the shock pulses and the enlarged HR-TEM image is presented in Fig. 6 and a similar kind of graphitization output is witnessed in the XRD as well as Raman results. Similar kind of morphological features under shocked conditions has been reported in Ref. [31]. The short-range ordered graphitic domains may contain hexagonal and pentagonal rings wherein the carbon atoms are located at the vertices forming two single bonds and one double bond with the neighboring carbon atoms with the presence of delocalized p-electrons across the molecule. The zoomed-in portions (Figs. S3–S5) of the HR-TEM images clearly represent the formation of short-range ordered graphitic domains under shocked conditions. In Fig. 6, HR-TEM images of the 750-shocked amorphous carbon sample are presented which also have the carbon onion structure similar to the 500-shocked condition whereas, at the 750-shocked condition, breaks could be observed between the carbon rings which may be because of the fragmentation of the carbon ring structures caused by the high lattice stress while the obtained XRD also reflect a similar trend in the results. For further understanding of the enhancement of the local structural order, the selected area electron diffraction (SAED) patterns of the control, 250, 500 and 750 shocked samples are provided in Fig. 7. As seen in Fig. 7a, the absence of the bright spots and diffused ring patterns demonstrate that the control sample belongs to the amorphous state, whereas under 250 and 500 shocked conditions, a slight enhancement of

the intensity of the diffused ring is witnessed which corresponds to the (002) plane and it demonstrates the formation of graphitic domains within the spheres. Notably, the 500-shocked sample's SAED patterns have slightly higher intensity compared to the 250-shocked sample's SAED pattern, which means that the 500-shocked sample has a higher concentration of graphitic domains within the spheres. At the 750-shocked condition, the intensity of the ring is reduced again because of the reduction in the graphitization, and the obtained features of the HR-TEM image are found to be well-matched with the XRD and Raman results.

#### 2.4. X-ray photoelectron spectroscopic analysis

X-ray photoelectron spectroscopic (XPS) data can provide additional information on the graphitization process of the carbon samples hence we have performed the XPS spectroscopic study for the control and shocked samples and the observed results are presented in Fig. 8. The control sample survey spectra are presented in Fig. 8a, and the spectral features of the control and shocked samples' core C1 s are presented in Fig. 8(b–e).

As seen in Fig. 8a, the control sample's C1 peak is fitted with three peaks which belong to C–C, C–O and C=O, respectively and the observed values of these peaks are found to be well-matched with the previous reports [48]. Note that, among the three peaks, the C–C peak can provide a possible understanding of the features of the local order and disorder of carbon and the C–C peak shift towards the lower binding energy which describes the formation of the graphitic particles [49,50]. The observed C–C peak positions are 284.69, 284.58, 284.53 and 284.61 eV for the control, 250, 500 and 750 shocked samples, respectively. Notably, the 500-shocked sample's C–C peak value has lower binding energy than the other samples which demonstrates that the 500-shocked sample has a higher concentration of graphitic domains [49,50].

#### 2.5. Magnetic properties

The carbon element does not belong to the magnetic element category and based on its atomic configuration, it belongs to the diamagnetic state such that, theoretically, all the crystalline allotropes such as graphite and diamond belong to the diamagnetic state [51]. But while referring to the experimental part, it is very difficult to achieve a perfect

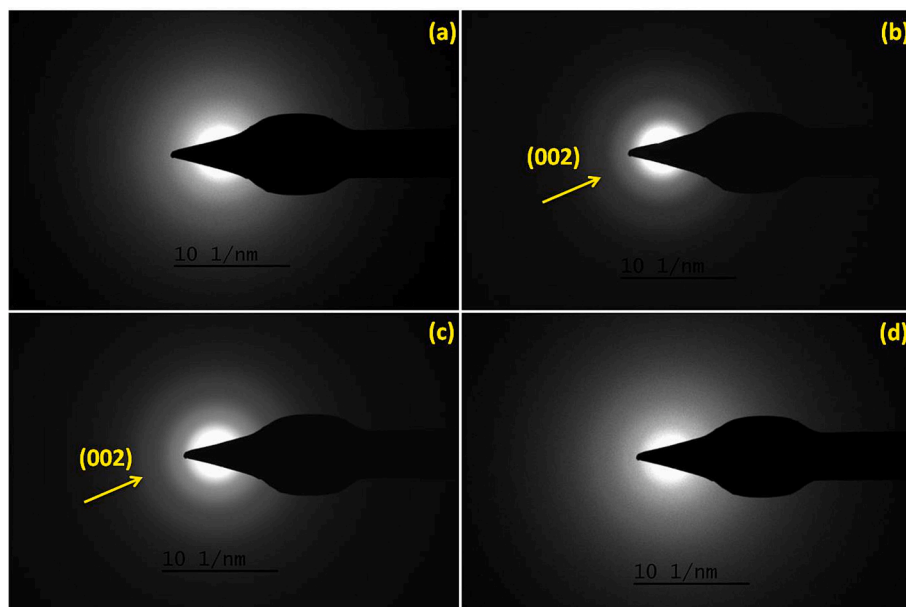


Fig. 7. SAED patterns of the control and shocked amorphous carbon samples (a) the control (b) 250 shocked (b) 500 shocked (c) 750 shocked conditions.

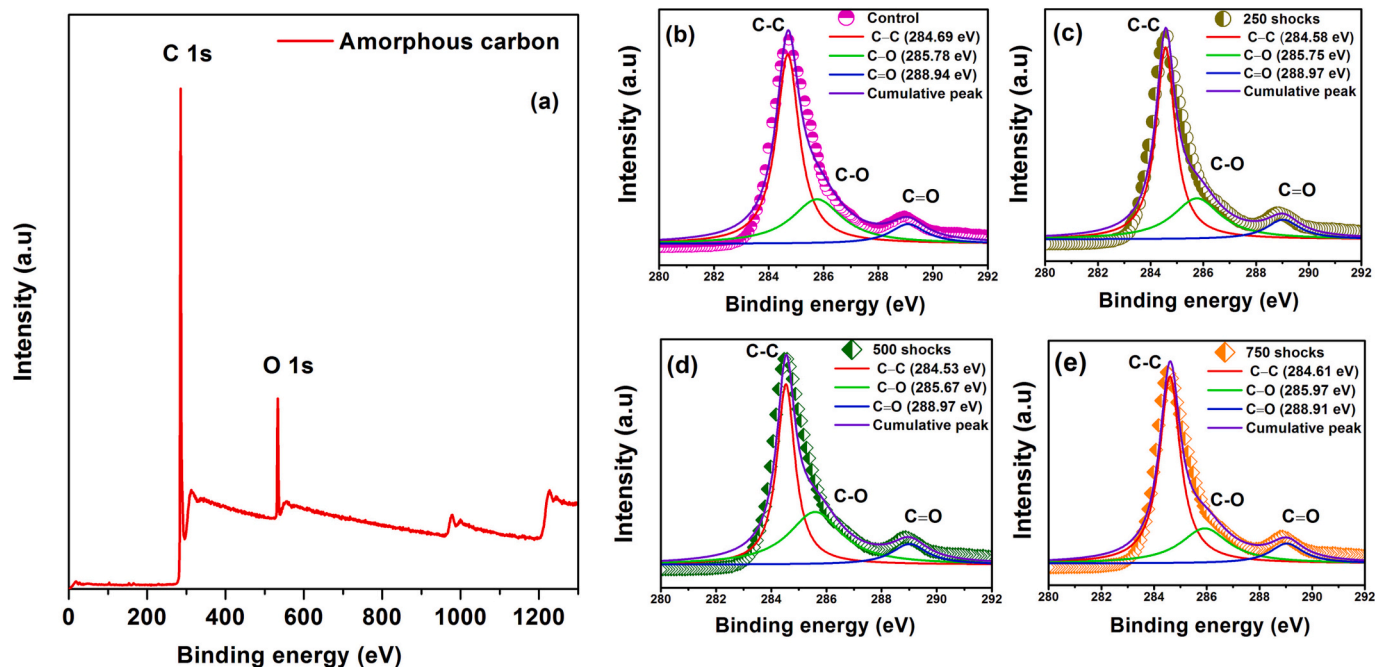


Fig. 8. XPS spectra of the control and shocked samples (a) survey spectra of the control sample (b) core C 1s spectrum of the control sample (c) core C 1s spectrum of the 250 shocked sample (d) core C 1s spectrum of the 250 shocked sample (e) core C 1s spectrum of the 750 shocked sample.

diamagnetic state of carbon material because of the presence of defects in carbon material whereby they tend to be highly sensitive to the magnetic field such that if materials have defects, they exhibit magnetic behavior based on the density of the defects [52]. After the experimental finding of the magnetic response in carbon-based materials, the understanding of magnetism in carbon materials has become an active research area. In addition to that, because of the magnetic responses of carbon, it is possible to draw a solid conclusion on the shock wave-induced graphitization on amorphous carbon materials so that vibrating sample magnetometer (VSM) has been utilized to study the magnetic behavior at room temperature and the obtained M-H loops of the control and shocked samples are presented in Fig. 9. As reflected in Fig. 9, the control sample has a high saturation magnetization and based on its hysteresis loop, it is tagged to be with the weak ferromagnetic state which is a good match with the previous results [39,52,53]. Note that the appearance of a weak ferromagnetic state may be due to the

presence of a large number of defects and non-hexagons in the control sample and also it is obviously connected to the existing number of weak ferromagnetic or paramagnetic spins. If the number of defects is high, the saturation magnetization is also high [53–55]. Under shocked conditions, the saturation magnetization reduces for the 250 and 500 shocked condition whereas it slightly increases at 750-shocked conditions (Fig. 9). However, all the shocked samples have the lower saturation magnetization values compared to the control sample. The reduction of the saturation magnetization for the shocked samples must be because of the formation of short-range ordered graphitic domains on the surface of the amorphous carbon sample and these results are found to be well-incorporated with the XRD, Raman, and TEM results of the sample.

In addition to that, the physical density of the non- $sp^2$  hybridizations must have a higher saturation magnetization because of the presence of high-level defects in the system. If the saturation magnetization is found to have reduced, the density of the sample must have reduced thereby the graphitization process must have occurred. Followed by the 500-shocked condition, at the 750-shocked condition, there is an increase in the value of saturation magnetization which is due to the fragmentation and bond length disorder of the graphitic lines in the carbon onion shells by the high threshold impact of the shock waves. The shock wave-induced strain reduces the fraction of  $\pi$  orbital overlapping on the neighboring atoms thereby allowing the system to sustain the high moment. For a better understanding of the relation between the degree of crystalline nature and saturation magnetization, in Fig. 10, the  $I_D/I_G$  intensity ratio and saturation magnetization values for the control and shocked samples are presented with respect to the number of shock pulses wherein both the parameters follow almost the similar kind of trend. Note that the  $I_D/I_G$  intensity ratio is reduced at 250-shocked condition such that  $sp^2$  carbon atoms significantly increase thereby resulting in the respective reduction in the saturation magnetization [53–55].

Following by  $I_D/I_G$  ratio, in Fig. 11, we have presented the data plot which related to relation between saturation magnetization and G-band shift with respect to number of shock pulses. Based on the obtained plots, the control sample has a smaller number of graphitic particles whereas under shocked conditions, the formation of the graphitic

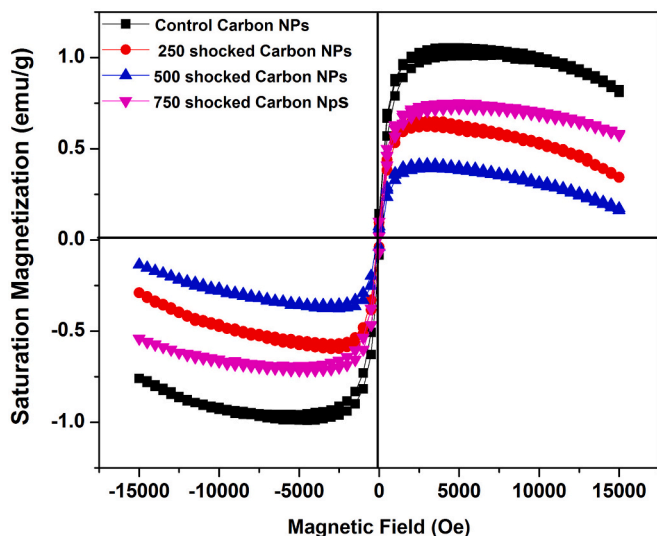
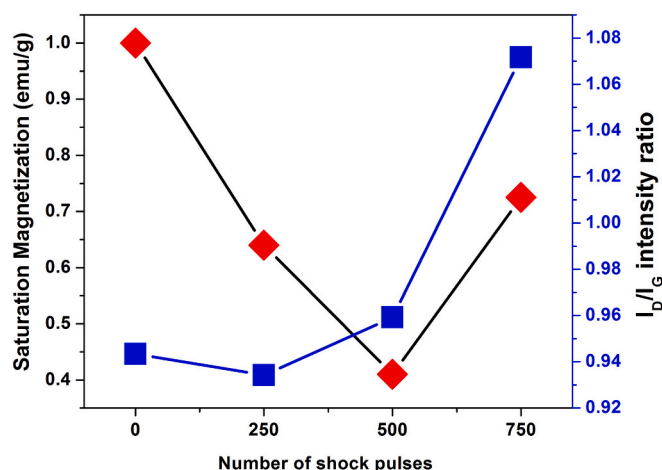


Fig. 9. VSM plots of the control and shocked amorphous carbon sample.



**Fig. 10.** Relation between the saturation magnetization and  $I_D/I_G$  intensity ratio of the amorphous carbon samples with respect to the number of shock pulses.

particles is considerably increased. Based on the obtained profile, the control sample has a higher saturation magnetization value due to the higher concentration of the defects whereas the lower saturation magnetization values of the shocked samples clearly demonstrate the formation of graphitic structures particularly at 500 shocked condition.

Furthermore, in Fig. 12, we have presented the plot which relates to the (002) diffraction peak positions and saturation magnetization values with respect to the number of shock pulses and the obtained plots are found to be well matched with the G-band shift and HR-TEM results.

### 3. Conclusion

In consolidating the findings of the present research work, the experimental results provide propounding insights into the practical issues of manufacturing carbon materials as well as the enlightenment of academic understanding of carbon chemistry at extreme conditions thereby it can be an asset for further studies. The fabrication of highly-ordered crystalline carbon materials is highly expensive and it is still

under the active domain of research. Using the acoustical shock wave-loading technique, the short-range ordered graphitic domains could be achieved from the amorphous carbon nanoparticles, and the successful transition is explained on the basis of the X-ray diffraction, Raman spectroscopic and HR-TEM techniques and the supporting shred of evidence is provided by the VSM analysis. Under shocked conditions, the occurrence of the artificial nucleation process is authenticated which leads to the short-range ordered graphitic domains whereby it is also found that the degree of the artificial nucleation process is highly dependent on the number of exposed shock pulses. According to the literature, a conventional shock tube capable of producing a 7300 K shock pulse is used to synthesize the crystalline spherical onions from the amorphous carbon. But in the present exploration, the breakthrough accomplishment is that a tabletop pressure-driven shock tube (Reddy Tube) capable of producing 864 K shock pulses is utilized for the synthesis of short-range ordered graphitic domains from the amorphous carbon samples. These results clearly disclose the understanding of the potential capability of the tabletop shock tube whereby the usage of such shock tubes can massively reduce the financial burden of the research institutions spread across the globe such that many more ground-breaking results would emerge in the near future.

#### Ethics approval

Not applicable.

#### Consent to participate

All the authors agree to participate.

#### Informed consent

All people involved in or responsible for the research are informed and consent.

#### CRedit authorship contribution statement

**Sivakumar Aswathappa** and **Lidong Dai** - conceptualized the project and Roles/Writing - original draft. **Sahaya Jude Dhas**

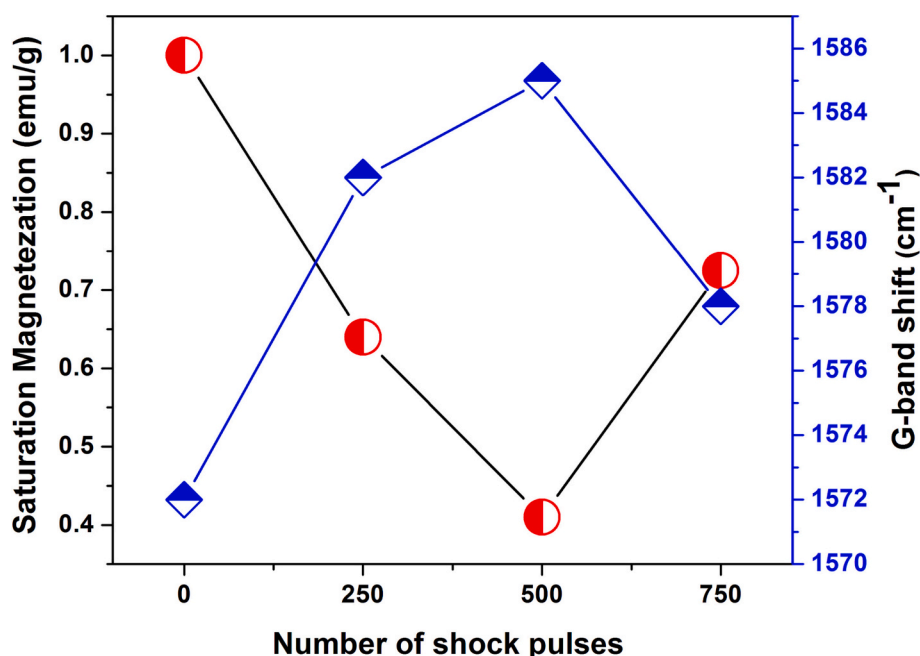


**Fig. 11.** Relation between the saturation magnetization and G-band shift of the amorphous carbon samples with respect to the number of shock pulses.

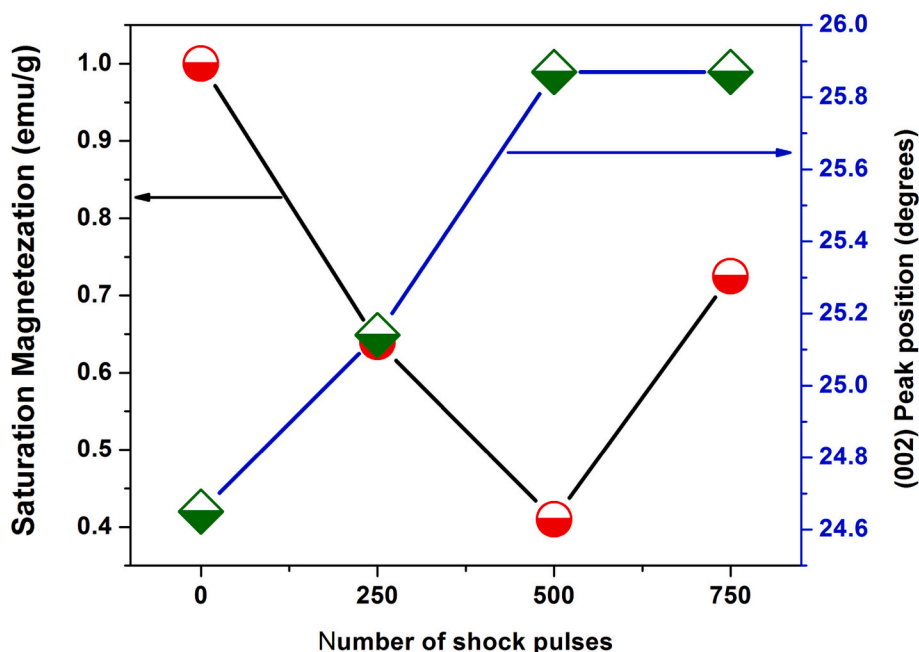


Fig. 12. Relation between the saturation magnetization and (002) peak positions of the amorphous carbon samples with respect to the number of shock pulses.

**Sathiyadhas**- Visualization, Roles/Writing - original draft. **Martin Britto Dhas Sathiyadhas Amalpushpam** - Investigation, Writing-review & editing. **Muthuvel Vijayan** and **Ikhyun Kim**- sample preparations and characterizations. **Raju Suresh Kumar** and **Abdulrahman I. Almansour** helped the data processing and analysis. All the authors discussed the results and commented on the manuscript.

#### Declaration of competing interest

The authors declare no conflict financial interests.

#### Data availability

The data that support the findings of this study are available from the corresponding author upon reasonable request.

#### Acknowledgment

The authors thank NSF of China (42072055). The project was supported by Researchers Supporting Project number (RSP2023R142), King Saud University, Riyadh, Saudi Arabia.

#### Appendix A. Supplementary data

Supplementary data to this article can be found online at <https://doi.org/10.1016/j.diamond.2023.110587>.

#### References

- [1] N. Koteeswara Reddy, V. Jayaram, E. Arunan, Y.B. Kwon, W.J. Moon, K.P.J. Reddy, Investigations on high enthalpy shock wave exposed graphitic carbon nanoparticles, *Diamond Relat. Mater.* 35 (2013) 53–57.
- [2] L. Biennier, V. Jayaram, N. Suas-David, R. Georges, M. Kiran Singh, E. Arunan, S. Kassi, E. Dartois, K.P.J. Reddy, Shock-wave processing of C<sub>60</sub> in hydrogen, *A&A* 599 (2017) 42.
- [3] Arijit Roy, Surendra Vikram Singh, M. Ambresh, D. Sahu, et al., Shock processing of amorphous carbon nanodust, *Adv. Space Res.* 70 (2022) 2571–2581.
- [4] A. Sivakumar, S. Sahaya Jude Dhas, T. Pazhanivel, Abdulrahman I. Almansour, Raju Suresh Kumar, Natarajan Arumugam, C. Justin Raj, S.A. Martin Britto Dhas, Phase transformation of amorphous to crystalline of multiwall carbon nanotubes by shock waves, *Cryst. Growth Des.* 21 (2021) 1617–1624.
- [5] Lidong Dai, Pu Chang, Heping Li, Hu Haiying, Kaixiang Liu, Linfei Yang, Meiling Hong, Characterization of metallization and amorphization for GaP under different hydrostatic environments in diamond anvil cell up to 40.0 GPa, *Rev. Sci. Instrum.* 90 (2019), 066103.
- [6] Meiling Guo, Xu Zhentao, Lei Yang, Xu Chaoyuan, Pengyang Li, Quandai Wang Zhenchao Yang, Mingshun Yang, Yan Li, A comparison between ion irradiation assisted- and electron irradiation assisted-oxygen plasma treatment on modification of nanostructured carbon films, *Surf. Coat. Technol.* 466 (2023), 129656.
- [7] Meiling Hong, Lidong Dai, Hu Haiying, Xinyu Zhang, Chuang Li, Yu He, Pressure-induced structural phase transition and metallization of CrCl<sub>3</sub> under different hydrostatic environments up to 50.0 GPa, *Inorg. Chem.* 61 (2022) 4852–4864.
- [8] C.C. Hwang, H.S. Kim, Y.K. Kim, K.W. Ihm, C.Y. Park, K.S. An, K.J. Kim, T.H. Kang, B. Kim, Temperature-induced reversible phase transition of a Si (113) surface, *Phys. Rev. B.* 64 (2001), 045305.
- [9] Elisabeta Horvath-Bordon, Ralf Riedel, Andreas Zerr, Paul F. McMillan, Gudrun Auffermann, Yuri Prots, Welf Bronger, Rudiger Knip, Peter Kroll, High-pressure chemistry of nitride-based materials, *Chem. Soc. Rev.* 35 (2006) 987–1014.
- [10] V.M. Egorova, P.N. Yakusheva, M.A. Arsentevb, A.S. Smolyanskii, The effect of gamma irradiation on phase transitions in polytetrafluoroethylene doped with silicon dioxide of plant origin, *Phys. Solid State* 62 (2020) 1506–1511.
- [11] Patrick Vanraes, Annemie Bogaerts, Laser-induced excitation mechanisms and phase transitions in spectrochemical analysis – review of the fundamentals, *Spectrochim. Acta Part B.* 179 (2021), 106091.
- [12] Amira Ben Gouider Trabelsi, V. Balasubramani, Fatemah H. Alkallas, A. Sivakumar, Mohd. Shkir, V. Manjunath, Si-Hyun Park, Investigation on effect of sintering temperature on structural, morphological and magnetic properties of pure and tin doped nickel ferrites for soft magnetic device applications, *Surf. Interfaces* 36 (2023), 102511.
- [13] Lu Xujie, Hu Qingyang, Wenge Yang, Ligang Bai, Howard Sheng, Lin Wang, Fuqiang Huang, Jianguo Wen, Dean J. Miller, Yusheng Zhao, Pressure-induced amorphization in single-crystal Ta<sub>2</sub>O<sub>5</sub> nanowires: a kinetic mechanism and improved electrical conductivity, *J. Am. Chem. Soc.* 135 (2013) 13947–13953.
- [14] R. Quesada Cabrer, A. Sella, E. Bailey, O. Leynaud, P.F. McMillan, High-pressure synthesis and structural behavior of sodium orthonitrate Na<sub>3</sub>NO<sub>4</sub>, *J. Solid State Chem.* 184 (2011) 915–920.
- [15] K.P.J. Reddy, N. Sharath, Manually operated piston-driven shock tube, *Curr. Sci.* 104 (2013) 172–174.
- [16] A. Sivakumar, S. Balachandar, S.A. Martin Britto Dhas, Measurement of “shock wave parameters” in a novel table-top shock tube using microphones, *Hum. Fact. Mech. Eng. Defen. Safety.* 4 (2020) 3.
- [17] A. Sivakumar, P. Eniya, S. Sahaya Jude Dhas, Abdulrahman I. Almansour, Raju Suresh Kumar, Natarajan Arumugam, J. Kalyana Sundar, Shubhadip Chakraborty, S.A. Martin Britto Dhas, Switchable phase transition of crystalline to amorphous state of potassium nitrate single crystal, *Surf. Interface* 35 (2022), 102422.
- [18] L. Anandaraaj, L. Jothi, Effect of shock waves on enhancing the optical properties of ammonium pentaborate hexahydrate single crystal molecular structure, *J. Mole. Struct.* 1233 (2021), 130068.
- [19] J.H. Joshi, S.A. Martin Britto Dhas, D.K. Kanchan, M.J. Joshi, K.D. Parikh, Dielectric relaxation and complex electrical formulation studies of shockwave-treated ammonium dihydrogen phosphate crystals, *J. Phys. Chem. Solid* 150 (2021), 109885.

- [20] Vishakantaiah Jayaram, Ravichandran Ranjith, Parthasarathi Bera, Non-catalytic behavior of SiO<sub>2</sub> fine powders in presence of strong shock waves for aerospace applications, *J. Mater. Sci. Appl.* 4 (2018) 37–46.
- [21] A. Sivakumar, S. Sahaya Jude Dhas, Shubhadip Chakraborty, Raju Suresh Kumar, Abdulrahman I. Almansour, Natarajan Arumugam, S.A. Martin Britto Dhas, Dynamic shock wave-induced amorphous-to-crystalline switchable phase transition of lithium sulfate, *J. Phys. Chem. C* 126 (2022) 3194–3201.
- [22] S. Kalaiarasi, A. Sivakumar, S.A. Martin Britto Dhas, M. Jose, Shock wave induced anatase to rutile TiO<sub>2</sub> phase transition using pressure driven shock tube, *Mater. Lett.* 219 (2018) 72–75.
- [23] A. Sivakumar, S. Sahaya Jude Dhas, P. Sivaprakash, Raju Suresh Kumar, Abdulrahman I. Almansour, Karthikeyan Perumal, S. Arumugam, S.A. Martin Britto Dhas, Shock wave induced reversible phase transition from crystalline to semi-crystalline states of lithium sulfate monohydrate, *J. Solid State Chem.* 307 (2022), 122859.
- [24] A. Sivakumar, A. Rita, S. Sahaya Jude Dhas, K.P.J. Reddy, Raju Suresh Kumar, I. Abdulrahman, D. Shubhadip Chakraborty Almansour, K. Moovendaran, Jayavel Sridharg, S.A. Martin Britto Dhas, Dynamic shock wave driven simultaneous crystallographic and molecular switching between  $\alpha$ -Fe<sub>2</sub>O<sub>3</sub> and Fe<sub>3</sub>O<sub>4</sub> nanoparticles – a new finding, *Dalton Trans.* 51 (2022) 9159–9166.
- [25] A. Sivakumar, S. Reena Devi, J. Thirupathy, R. Mohan Kumar, S.A. Martin Britto Dhas, Effect of shock waves on structural, thermophysical and dielectric properties of glycine phosphate (GPI) crystal, *J. Elect. Mater.* 48 (2019) 7216–7225.
- [26] A. Sivakumar, S. Suresh, J. Anto Pradeep, S. Balachandar, S.A. Martin Britto Dhas, Effect of shock waves on dielectric properties of KDP crystal, *J. Electron. Mater.* 47 (2018) 4831–4839.
- [27] V. Mowlika, C.S. Naveen, A.R. Phani, A. Sivakumar, S.A. Martin Britto Dhas, R. Robert, Shock wave induced magnetic phase transition in cobalt ferrite nanoparticles, *Mater. Chem. Phys.* 275 (2022), 125300.
- [28] A. Rita, A. Sivakumar, S. Sahaya Jude Dhas, S.A. Martin Britto Dhas, Reversible magnetic phase transitions of MnO<sub>2</sub> nano rods by shock wave recovery experiments, *J. Mater. Sci. Mater. Electron.* 31 (2020) 20360–20367.
- [29] Travis J. Volz, Y.M. Gupta, Graphite to diamond transformation under shock compression: role of orientational order, *J. Appl. Phys.* 125 (2019), 245902.
- [30] Paul S. Decarli, John C. Jamieson, Formation of diamond by explosive shock, *Science* 133 (1961) 1821–2822.
- [31] D.J. Erskine, W.J. Nellies, Shock induced martensitic phase transformation of oriented graphite to diamond, *Nature* 349 (1991) 317–319.
- [32] A.V. Kurdyumov, V.F. Britun, V.V. Yarosh, A.I. Danilenko, V.B. Zelyavskii, The influence of the shock compression conditions on the graphite transformations into lonsdaleite and diamond, *J. Superhard. Mater.* 34 (2012) 19–27.
- [33] Hu Meng, Julong He, Zhisheng Zhao, Timothy A. Strobel, et al., Compressed glassy carbon: an ultrastrong and elastic interpenetrating graphene network, *Sci. Adv.* 3 (2017) 1603213.
- [34] M. Moseler, H. Riedel, P. Gumbsch, J. Staring, B. Mehlhig, Understanding of the phase transformation from fullerite to amorphous carbon at the microscopic level, *Phys. Rev. Lett.* 94 (2005), 165503.
- [35] A.C. Ferrari, J. Robertson, Interpretation of Raman spectra of disordered and amorphous carbon, *Phys. Rev. B* 61 (2000) 095.
- [36] A.M. Molodetsa, A.A. Golyshev, Structural transformations of amorphous carbon (glassy carbon) at high shock pressures, *J. Exp. Theor.* 126 (2018) 772–778.
- [37] A.F. Goncharov, Graphite at high pressures: amorphization at 44 GPa, *High Press. Res* 8 (1992), 607416.
- [38] Akifumi Onodera, Koji Higashi, Yasushi Irie, Crystallization of amorphous carbon at high static pressure and high temperature, *J. Mater. Sci.* 23 (1988) 422–428.
- [39] Anton Komlev, Erkki Lähderanta, Evgeniy Shevchenko and Nikolay Vorobev Desyatovskii, Magnetism of purified amorphous carbon, *EPJ Web of Conf.* 185 (2018) 04012.
- [40] Caiyun Zhang, Xiaohong Zhu, Zhongxing Wang, Ping Sun, Yinjuan Ren, Jiliang Zhu, Jianguo Zhu, Dingquan Xiao, Facile synthesis and strongly microstructure-dependent electrochemical properties of graphene/manganese dioxide composites for supercapacitors, *Nano. Res. Lett.* 9 (2014) 490.
- [41] Azam Marjani, Ali Taghvaei Nakhjiri, Maryam Adimi, Hassan Fathinejad Jirandehi, Saeed Shirazian, Effect of graphene oxide on modifying polyethersulfone membrane performance and its application in wastewater treatment, *Sci. Rep.* 10 (2020) 2049.
- [42] D.G. Morris, An investigation of the shock induced transformation of graphite to diamond, *J. Appl. Phys.* 51 (1980) 2059.
- [43] Zihe Li, Yujia Wang, Mengdong Ma, Huachun Ma, et al., Ultrastrong conductive in situ composite composed of nanodiamond incoherently embedded in disordered multilayer graphene, *Nat. Mater.* 22 (2023) 42–49.
- [44] Sheng-cai Zhu, Xiao-zhi Yan, Liu Jin, Artem R. Oganov, Qiang Zhu, A revisited mechanism of the graphite-to diamond transition at high temperature, *Matter* 3 (2020) 1–15.
- [45] T. Kim, L. Jaeger, L. Kun-Hong, Full graphitization of amorphous carbon by microwave heating, *RSC Adv.* 6 (2016) 24667–24674.
- [46] M.A. Pimenta, G. Dresselhaus, M.S. Dresselhaus, L.G. Cancado, A. Jorio, R. Saito, Studying disorder in graphite-based systems by Raman spectroscopy, *Phys. Chem. Chem. Phys.* 9 (2007) 1276–1291.
- [47] J. Gaudin, O. Peyrusse, J. Chalupsky, M. Toufarova, et al., Amorphous to crystalline phase transition in carbon induced by intense femtosecond X-ray free-electron laser pulses, *Phy. Rev. B.* 86 (2012), 024103.
- [48] Kangsen Li, Xu Gang, Xiaobin Wen, Jun Zhou, Feng Gong, High-temperature friction behavior of amorphous carbon coating in glass molding process, *Friction* 9 (2021) 1648–1659.
- [49] C. Xiangnan, W. Xiaohui, F. De, A review on C1s XPS-spectra for some kinds of carbon materials, *Fuller. Nanotub. Carbon Nanostructures.* 28 (2020) 1048–1058.
- [50] Ayaka Fujimoto, Yasuhiro Yamada, Michio Koinuma, Satoshi Sato, Origins of sp<sup>3</sup>C peaks in C 1s X-ray photoelectron spectra of carbon materials, *Anal. Chem.* 88 (2016) 6110–6114.
- [51] N.V. Balam Thakur, Chandra Shekar, Sharat Chandra, Sujay Chakravarty, Effect of sp hybridization and bond-length disorder on magnetism in amorphous carbon—a first-principles study, *Diamond Relat. Mater.* 121 (2022), 108725.
- [52] C.N.R. Rao, H.S.S. Ramakrishna Matte, K.S. Subrahmanyama, Urmimla Maitra, Unusual magnetic properties of graphene and related materials, *Chem. Sci.* 3 (2012) 45.
- [53] S.K. Sarkar, K.K. Raul, S.S. Pradhan, S. Basu, A. Nayak, Magnetic properties of graphite oxide and reduced graphene oxide, *Physica E* 64 (2014) 78–82.
- [54] Ana Elisa Ferreira Oliveira, Guilherme Bettio Braga, Cesar Ricardo Teixeira Tarley, Arnaldo Cesar Pereira, Thermally reduced graphene oxide: synthesis, studies and characterization, *J. Mater. Sci.* 53 (2018) 12005–12015.
- [55] A. Sivakumar, S. Lidong Dai, Sahaya Jude Dhas, S.A. Martin Britto Dhas, V. Mowlika, Raju Suresh Kumar, Abdulrahman I. Almansour, Reduction of amorphous carbon clusters from the highly disordered and reduced graphene oxide NPs by acoustical shock waves — towards the formation of highly ordered graphene, *Diamond Relat. Mater.* 137 (2023), 110139.